Using numerical continuation to study "large" amplitude solutions to the 2:1 forced complex Ginzburg–Landau equation

October 7, 2014

Boston University/ Keio University Dynamical Systems Workshop 2014
Lecture notes for Kelly McQuighan

1 Review of numerical continuation [11]

See the lecture notes [11] for more details. We are interested in problems of the form

$$U_t = F(U;\mu) \quad U \in \mathbb{R}^n,\ \mu\mathbb{R}$$

where μ is a parameter. For example, consider

$$u_t = -\mu + u^2, u \in \mathbb{R}. \tag{1.1}$$

Suppose that we are interested in steady state solutions to (1.1). One can easily see that such solutions satisfy $u^2 = \mu$. Thus,

$$u = \begin{cases} \pm\sqrt{\mu} & \mu \geqslant 0 \\ DNE & \mu < 0 \end{cases}$$

Thus, steady state solutions depend on the parameter μ.

The idea behind continuation is to try to use information about known solutions to find "nearby" solutions. This is possible by the implicit function theorem. For example, to find steady state solutions to equation (1.1), we look for zeros of the function $f(u;\mu) := u^2 - \mu$. Suppose that we know the exact solution $u = u^*$ for a fixed $\mu = \mu^*$; then it must be true that $f(u^*;\mu^*) = 0$. One can easily check that $f_u(u^*;\mu^*) \neq 0$ provided $u \neq 0$; thus, by the implicit function theorem, there exists function $g(\mu)$ for μ near μ^* so that $f(g(\mu);\mu) = 0$. The curve $g(\mu)$ is the curve of equilibria in parameter space; see Figure 1. This means that to perform numerical continuation we need a method of finding zeros of functions.

1.1 Newton's method

Consider $f^\mu(u) := f(u;\mu)$ with μ fixed. We assume for convenience that $f : \mathbb{R} \to \mathbb{R}$. We are interested in finding the value of u so that $f^\mu(u) = 0$. We take as our initial guess $u_0 := u^*$ where $f(u^*;\mu^*) = 0$ and μ is very close to μ^*. Then our next guess u_1 is computed by finding the intersection of the tangent line to f^μ at u_0 with the $u = 0$ axis; see Figure 2. In particular,

$$u_1 = u_0 - \frac{f(u_0)}{f_u(u_0)}.$$

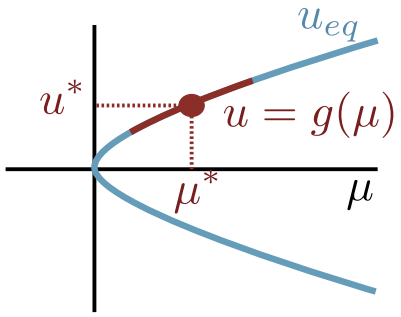

Figure 1: *Existence of equilibrium solutions for μ near μ^*. The curve of such solutions is given by $g(\mu)$, where $g(\mu)$ exists due to the implicit function theorem.*

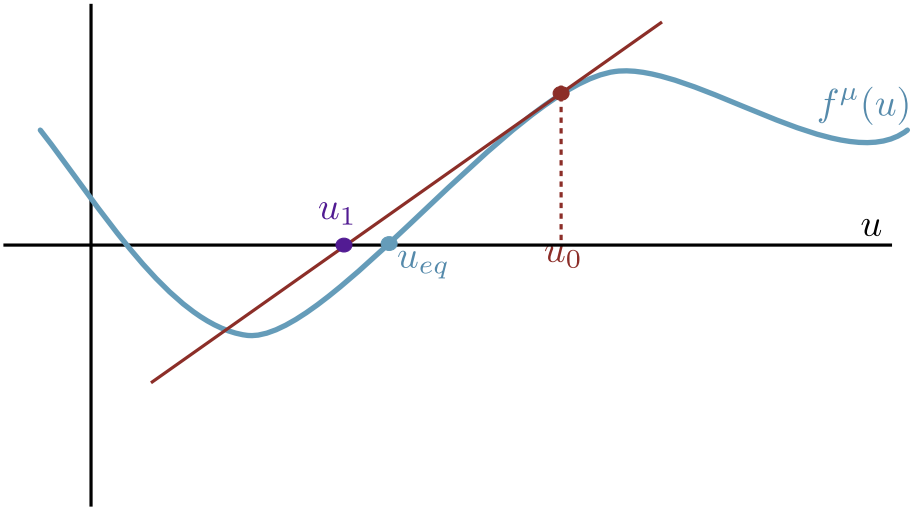

Figure 2: *Step 1 of Newton's method to find zeros of $f^\mu(u)$.*

One then repeats the process to find successive guesses for u_{eq}:

$$u_{n+1} = u_n - \frac{f(u_n)}{f_u(u_n)}.$$

and one can show that $u_n \to u_{eq}$ as $n \to \infty$.

For numerical continuation, the procedure is as follows. We are interested in computing the curve of parameter-dependent equilibria $\{U : F(U) = 0\}$ where $U = (u, \mu)$. We assume that we know one point on the curve $U^* = (u^*, \mu^*)$. We compute the tangent to the curve of equilibria at U^* by finding $\{V_* : F_U(U^*)V_* = 0\}$. We take a small step $h \ll 1$ along this tangent space; this is our initial guess for Newton's method. We then perform Newton's method on the subspace which is perpendicular to the tangent space $\{U : \langle U - U^*, V_* \rangle = h, ||V_*|| = 1\}$. See Figure 3.

A very good numerical continuation package exists known as AUTO07p [4].

2 Our problem: Experimental observation of oscillons [8]

The motivation for this talk is oscillons: spatially localized, temporally oscillating structures that emerge from a uniform background state in parametrically forced nonlinear systems.

Oscillons were first observed in an experiment performed by Umbanhowar et al. using granular media [13]. In that work, the researchers filled a 127 mm diameter circular disk with an approximately 3 mm thick layer of bronze

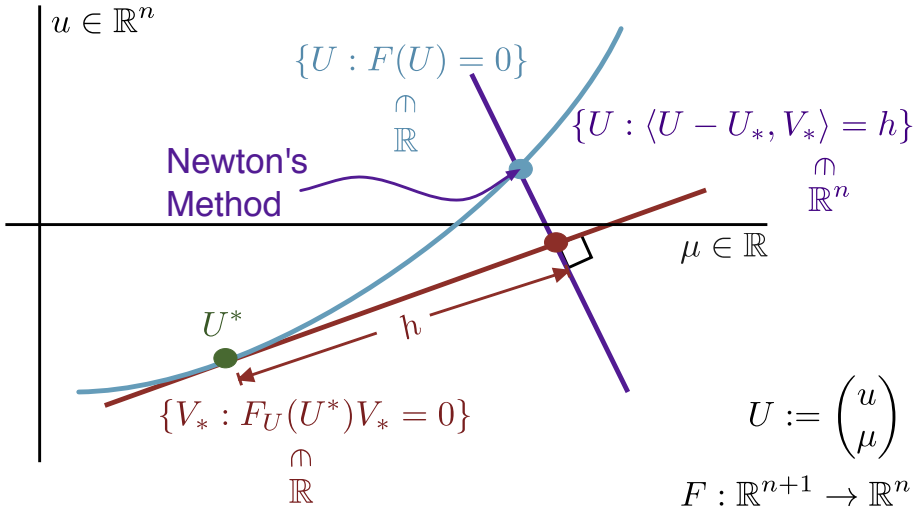

Figure 3: *Using Newton's method for numerical continuation. The blue curve is the curve of parameter dependent equilibria, which we would like to find. We assume that we know one point on this curve U^*. We perform Newton's method on the subspace $\{U : \langle U - U^*, V_* \rangle = h, ||V_*|| = 1\}$ with $U = U^* + hV_*$, $||V_*|| = 1$, as our initial guess.*

spheres. The bronze spheres were approximately 0.15-0.18 mm in diameter, so that the layer was approximately 17 spheres thick. The circular disk was then placed on a vibrating table and subjected to vertical vibrations. Oscillating heaps of beads were seen to emerge for certain values of the forcing frequency and amplitude. These heaps were seen to oscillate between a heap and a crater at half the forcing frequency; see Figure **??**. The oscillons were observed in a variety of arrangements; see Figure 4.

Oscillons were subsequently observed in a variety of experimental settings including Newtonian fluids [1, 12, 18, 19], chemical reactions [10, 15, 17], and colloidal suspensions [7]. In chemical reactions, oscillons have also been observed in autonomous systems [14] and in systems subjected to global feedback [16]. The frequency of the pattern oscillation is often close to the forcing frequency or half the forcing frequency, and we refer to these patterns as 1:1 and 2:1 resonance oscillons, respectively. See Figure 5 for some examples.

3 2:1 forced complex Ginzburg–Landau equation

We model the systems in which oscillons have been observed with the 2:1 forced complex Ginzburg–Landau (CGL) equation. We first explain the derivation and relevance of this equation to our problem. We then review known results on the 2:1 forced CGL in one space dimension; we are interested in the planar case.

3.1 Derivation [8]

We illustrate the derivation of the forced CGL for general forced systems by studying this issue in the context of forced reaction–diffusion systems. The details of this derivation are shown as part of [8]. We summarize the main ideas. We consider a periodically forced parameter dependent reaction–diffusion system

$$u_t = \Delta u + f(u; \nu) + \Gamma e^{2i\Omega t}, \quad u \in \mathbb{R}^m, \tag{3.1}$$

with Γ, Ω, $\nu \in \mathbb{R}$. We assume $f(0; \nu) = 0$ for all ν so that equation (3.1) supports the homogeneous rest solution $u(x, t) \equiv 0$. It has been argued, see for instance [3, 5], that the 2:1 forced complex Ginzburg–Landau (CGL) equation

$$A_T = (1 + i\alpha)\Delta A + (-\mu + i\omega)A - (1 + i\beta)|A|^2 A + \gamma \overline{A}, \quad A \in \mathbb{C} \tag{3.2}$$

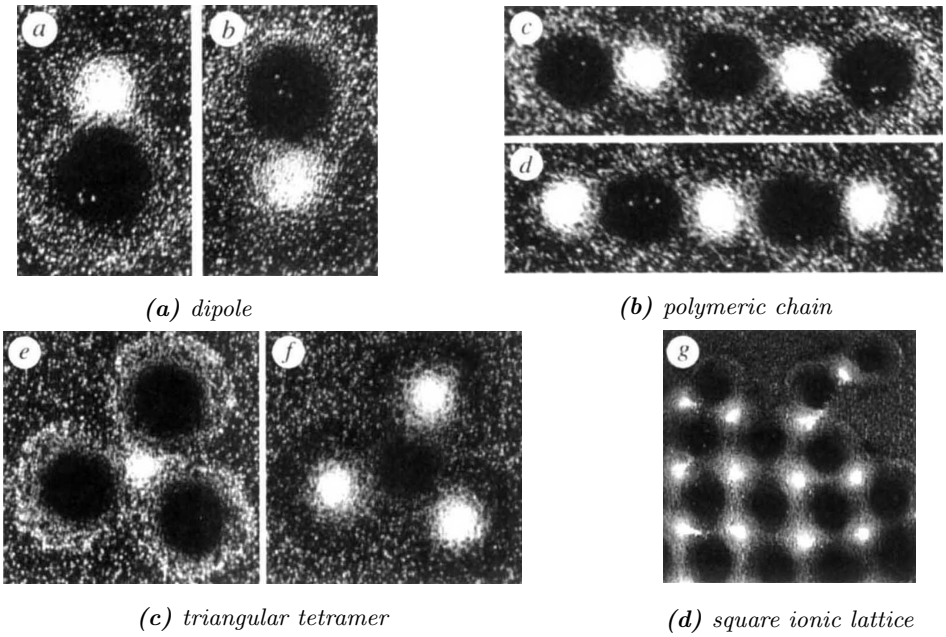

(a) *dipole* ***(b)*** *polymeric chain*

(c) *triangular tetramer* ***(d)*** *square ionic lattice*

Figure 4: *Top view of various arrangements of oscillons in a granular system. The system was illuminated from above so that the bright spots correspond with heaps and the dark spots correspond with craters. The time between the panels in Figures a-c is one forcing period. Figure taken from [13, Figure 3].*

is a modulation equation for (3.1) near a supercritical Hopf bifurcation of the rest state $u = 0$. In other words, $A(X, T)$ captures the "slow" dynamics of the envelope for a carrier wave evolving on the fast time scale t; see Figure 6. If the slow and fast scales could be completely separated, then one could write

$$u(t; X, T) = \epsilon A(X, T)e^{\mathrm{i}\Omega t}, \tag{3.3}$$

with $X := \epsilon x$ and $T := \epsilon^2 t$. The 2:1-ratio between the oscillation frequency of the forcing in (3.1) to that of the ansatz (3.3) is consistent with experimental findings. In equation (3.2), α, β, μ, ω, $\gamma \in \mathbb{R}$ are real parameters which can be obtained from the original equation (3.1). In this section we use a multiple scales analysis to formally derive (3.2) as the amplitude equation for (3.1). We remark that since the ansatz (3.3) explicitly factors out the time oscillations, oscillons correspond with localized steady state solutions to (3.2); i.e., spatially localized solutions to

$$0 = (1 + \mathrm{i}\alpha)\Delta A + (-\mu + \mathrm{i}\omega)A - (1 + \mathrm{i}\beta)|A|^2 A + \gamma\overline{A}, \quad A \in \mathbb{C}.$$

3.1.1 Hypotheses

We assume that the unforced reaction–diffusion system

$$u_t(x, t) = D\Delta u(x, t) + f(u(x, t); \nu), \quad u \in \mathbb{R}^m,\ x \in \mathbb{R}^n \tag{3.4}$$

supports a homogeneous rest solution $u(x, t) = u_0$ so that $f(u_0, \nu) = 0$ for all ν; without loss of generality, we assume $u_0 = 0$. We assume that f is smooth in both u and ν so that we can Taylor expand

$$f(u, \nu) = f_u(0; 0)u + N_2[u, u] + N_3[u, u, u] + f_\nu(0; 0)\nu + f_{u\nu}(0; 0)u\nu + \ldots \tag{3.5}$$

where $N_2[\ldots]$ and $N_3[\ldots]$ are the appropriate bilinear and trilinear forms. In what follows, we consider only isotropic solutions to (3.4) so that we can take $n = 1$ without loss of generality.

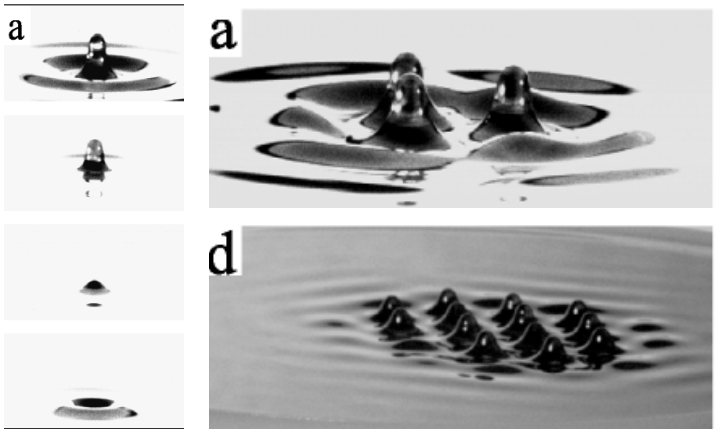

(a) *Newtonian fluid. The left panel is the time sequence for a single oscillon. The right two panels represent two different configurations of oscillons at a single snapshot in time. Figure taken from [1, Figures 1 and 2].*

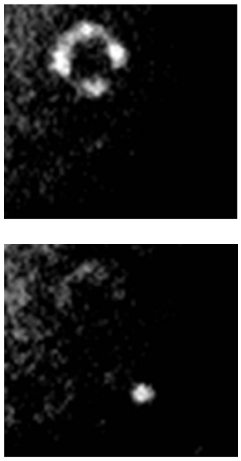

(b) *Belousov–Zhabotinsky chemical reaction. Time between panels equals the forcing period. Figure taken from [15, Figure 2].*

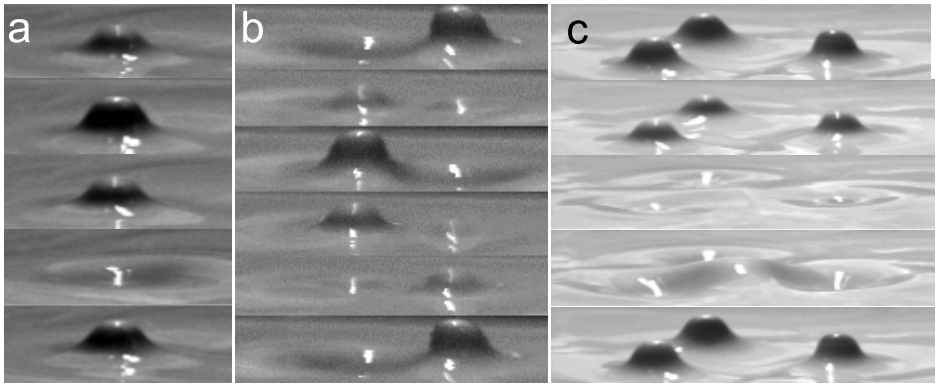

(c) *Colloidal suspension. The time sequence for three different configurations are shown: a single oscillon, a pair of oscillons, and an oscillon triad. Two full driving periods are shown for each sequence. Figure taken from [7, Figure 1].*

Figure 5: *Oscillons observed in other materials.*

We furthermore assume that $u = 0$ is a stable solution of (3.4) for $\nu > 0$ and that it undergoes a supercritical Hopf bifurcation as ν is decreased through zero. This last assumption is necessary so that equation (3.4) supports temporally oscillating solutions. In other words, we assume that the curves $\lambda = \lambda_\pm(k;\nu)$ which satisfy $d(\lambda_\pm(k;\nu), \mathrm{i}k;\nu) = 0$ cross the imaginary axis with nonzero speed at $\lambda = \pm\mathrm{i}\omega_0$, $\omega_0 \neq 0$, as ν is decreased through zero. See Figure 7. In the above,

$$d(\lambda, \Theta; \nu) := \det[\Theta^2 D + f_u(0;\nu) - \lambda], \quad \Theta \in \mathbb{C} \tag{3.6}$$

is the dispersion relation associated with $\partial_t u = \mathcal{L}u$, where $\mathcal{L}(\nu) := D\Delta + f_u(0;\nu)$, is the linearization of the unforced reaction–diffusion equation (3.4) about $u = 0$. The crossing of the essential spectrum through the imaginary axis leads to what is known as a Hopf bifurcation; this bifurcation can lead to either a stable (supercritical) or an unstable (subcritical) limit cycle. We assume that the cycle is stable; see Figure 8.

Lastly, we assume $\lambda = \pm\mathrm{i}\omega_0$ are simple eigenvalues for $f_u(0;0)v_0 = \lambda v_0$.

Under these hypotheses we add near 2:1 resonant forcing to (3.4) for $\nu =: \epsilon^2\widehat{\mu}$ small

$$u_t(x,t) = D\Delta u(x,t) + f(u(x,t), \epsilon^2\widehat{\mu}) + \epsilon^2\widehat{\gamma} v e^{2\mathrm{i}(\omega_0 - \epsilon^2\widehat{\omega})t}. \tag{3.7}$$

The parameters $\widehat{\mu}$, $\widehat{\gamma}$ and $\widehat{\omega}$ are real and bounded. The vector $v \in \mathbb{R}^m$ allows the amplitude of forcing to be

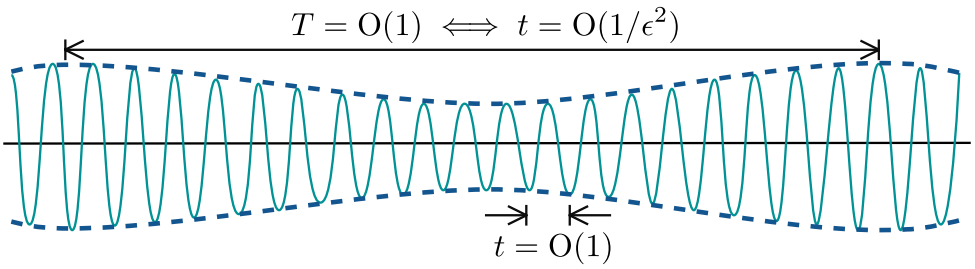

Figure 6: *Representation of the slow versus fast time scales in the multiple scales expansion. The solid teal line represents the carrier wave $u(x,t)$; it evolves over the fast time scale t. The dotted navy line represents the solution envelope $A(X,T)$; it evolves over the slow time scale $T := \epsilon^2 t$.*

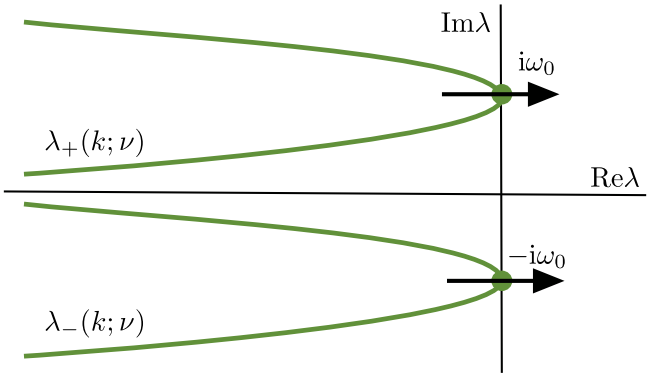

Figure 7: *Essential spectrum for $\mathcal{L}$, the unforced reaction–diffusion equation, linearized about $u = 0$. We assume that the essential spectrum of $\mathcal{L}$ crosses the imaginary axis with nonzero speed as ν is decreased through zero.*

different for each system variable. The scalings $\nu = \epsilon^2\widehat{\mu}$, $\epsilon^2\widehat{\gamma}$, and $\epsilon^2\widehat{\omega}$ are necessary for consistency in the scaling.

3.1.2 Multiple scales expansion set-up

We use a multiple scales expansion to model the evolution of small amplitude solutions to (3.7). This idea is explained further in, for example, [6, Chapter 7]. We define $X := \epsilon x$ and $T := \epsilon^2 t$. As shown in Figure 6, X and T capture the solution envelope as it evolves over the "long" space and "slow" time scales. We assume that the evolution of u on each time or space scale is independent of the other scales, i.e., $u = (x,t;X,T) = a(x,t)A(X,T)$. Since X and T depend implicitly on x and t, respectively, the derivatives in (3.7) become

$$\partial_t u(x,t;X,T) \mapsto \frac{\partial u}{\partial t} + \epsilon^2 \frac{\partial u}{\partial T} =: u_t + \epsilon^2 u_T \tag{3.8a}$$

and

$$\Delta u(x,t;X,T) \mapsto \frac{\partial^2 u}{\partial x^2} + \epsilon^2 \frac{\partial^2 u}{\partial X^2} =: \Delta_x u + \epsilon^2 \Delta_X u.$$

On the short space scale $\Delta_x u = 0$; we therefore write $u = u(t;X,T)$ and the spatial Laplacian operator Δ becomes

$$\Delta u(t;X,T) \mapsto \epsilon^2 \Delta_X u. \tag{3.8b}$$

One can see from the derivatives (3.8) that the relative scaling of X and T ensures that both slow variables affect u over the same scale $\mathrm{O}(1/\epsilon^2)$.

(a) *Supercritical Hopf bifurcation, $c_1 < 0$.* ***(b)*** *Subcritical Hopf bifurcation, $c_1 > 0$.*

Figure 8: *Supercritical versus subcritical Hopf bifurcation. Plotted is the radius of the cycle r versus the parameter ν. The zero solution exists for all ν. A limit cycle with $r > 0$ bifurcates at $\nu = 0$; it exists for either positive or negative ν, depending on the sign on c_1. Solid lines represent stable solutions whereas dotted lines represent unstable solutions.*

We plug the Taylor expansion (3.5) and derivatives (3.8) into equation (3.7) to get

$$\begin{aligned} u_t - f_u(0;0)u = &-\epsilon^2 u_T + \epsilon^2 D\Delta_X u + N_2[u,u] + N_3[u,u,u] \\ &+ \epsilon^2 f_{u\nu}(0;0)u\widehat{\mu} + \ldots + \epsilon^2\widehat{\gamma}ve^{2\mathrm{i}\omega_0 t}e^{-2\mathrm{i}\omega T}. \end{aligned} \tag{3.9}$$

Next, we expand solutions to (3.9) near $u = 0$

$$u(t;X,T) = \epsilon u_1(t;X,T) + \epsilon^2 u_2(t;X,T) + \epsilon^3 u_3(t;X,T) + c.c + \mathrm{O}(\epsilon^4). \tag{3.10}$$

We match terms in (3.9) at successively higher orders in ϵ.

$$\mathrm{O}(\epsilon): \quad \mathcal{L}_0 u_1 = 0 \tag{3.11a}$$

$$\mathrm{O}(\epsilon^2): \quad \mathcal{L}_0 u_2 = N_2[u_1,u_1] + \widehat{\gamma}ve^{2\mathrm{i}\omega_0 t}e^{-2\mathrm{i}\omega T} \tag{3.11b}$$

$$\mathrm{O}(\epsilon^3): \quad \mathcal{L}_0 u_3 = -\partial_T u_1 + D\Delta_X u_1 + 2N_2[u_1,u_2] + N_3[u_1,u_1,u_1] + \widehat{\mu}f^0_{u\nu}u_1 \tag{3.11c}$$

$$\vdots \qquad\qquad \vdots$$

where $\mathcal{L}_0 := \partial_t - f_u(0;0)$ is defined as a map

$$\mathcal{L}_0 : L^2([0,2\pi/\omega_0]/\sim) \to L^2([0,2\pi/\omega_0]/\sim),$$

with $\mathrm{dom}(\mathcal{L}_0) = H^1([0,\frac{2\pi}{\omega_0}]/\sim)$. In equations (3.11), the expressions f^0_ν and $f^0_{u\nu}$ are shorthand for the Taylor expansion vector $f_\nu(0;0)$ and matrix $f_{u\nu}(0;0)$, respectively.

3.1.3 Matching

We first solve (3.11a). By hypothesis the only nontrivial solutions to $\mathcal{L}_0 v(t) = 0$ are linear combinations of $e^{\mathrm{i}\omega_0 t}v_0$ and $e^{-\mathrm{i}\omega_0 t}\overline{v}_0$. Hence, $u_1 = A_1(X,T)e^{\mathrm{i}\omega_0 t}v_0 + c.c.$ with $A_1(X,T) \in \mathbb{C}$, and where A_1 is unknown. We can similarly solve the for u_2 using the $\mathrm{O}(\epsilon^2)$ terms. At $\mathrm{O}(\epsilon^3)$ we use the expressions for u_1 and u_2 in combination with the Fredholm alternative to find that $A_1(X,T)$ must satisfy

$$\begin{aligned} \partial_T A_1 v_0 \cdot w_0 = &\Big\{ \Delta_X A_1 D v_0 + \widehat{\mu}A_1 f^0_{u\nu}v_0 \\ &+ |A_1|^2 A_1 \big(-4N_2\left[v_0, (f^0_u)^{-1}N_2[v_0,\overline{v_0}]\right] \\ &+ 2N_2\left[\overline{v}_0, (2\mathrm{i}\omega_0 I - f^0_u)^{-1}N_2[v_0,v_0]\right] + 3N_3[v_0,v_0,\overline{v}_0]\big) \\ &+ 2\widehat{\gamma}\overline{A}_1 e^{-2\mathrm{i}\widehat{\omega}T}N_2[\overline{v}_0, (f^0_u - 2\mathrm{i}\omega_0 I)^{-1}v]\Big\} \cdot w_0, \end{aligned} \tag{3.12}$$

where v_0 and w_0 are eigenvectors corresponding with $\mathcal{L}_0$ and $\mathcal{L}_0^\dagger$, respectively; they are unique by hypothesis.

We remark that there exists appropriate coordinate transformations to turn (3.12) into the 2:1 forced complex Ginzburg–Landau equation

$$A_T = (1+\mathrm{i}\alpha)\Delta_X A + (-\mu + \mathrm{i}\omega)A - (1+\mathrm{i}\beta)|A|^2 A + \gamma\overline{A}. \tag{3.13}$$

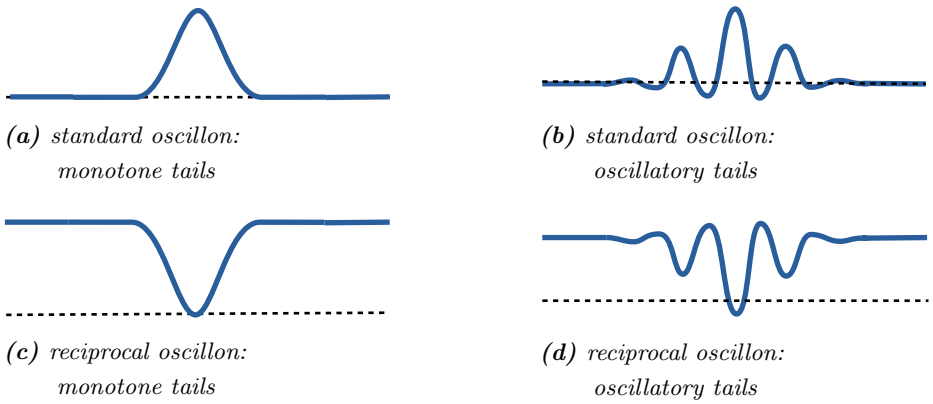

(a) *standard oscillon: monotone tails*

(b) *standard oscillon: oscillatory tails*

(c) *reciprocal oscillon: monotone tails*

(d) *reciprocal oscillon: oscillatory tails*

Figure 9: *Localized solutions to equation (3.15). The dotted line represents* $u \equiv 0$.

3.2 Review of results in 1 spatial dimension [2]

As discussed above, the 2:1 forced complex Ginzburg–Landau (CGL) equation

$$u_t = (1 + \mathrm{i}\alpha)\Delta u + (-\mu + \mathrm{i}\omega)u - (1 + \mathrm{i}\beta)|u|^2 u + \gamma\overline{u}, \quad u \in \mathbb{C} \tag{3.14}$$

captures the dynamics of small amplitude oscillatory solutions. Thus, oscillons correspond with steady state solutions to (3.14). In this section, we review known results for the steady state CGL in one space dimension

$$0 = (1 + \mathrm{i}\alpha)u_{xx} + (-\mu + \mathrm{i}\omega)u - (1 + \mathrm{i}\beta)|u|^2 u + \gamma\bar{u}, \quad u \in \mathbb{C},\ x \in \mathbb{R} \tag{3.15}$$

from [2]. We remark that in equations (3.14) and (3.15) we have used u as the amplitude variable, rather than A as in equation (3.2); this is for consistency with our notation throughout the remainder of these notes.

It was shown in [2] that (3.15) supports two types of localized solutions. The first localized solution, referred to as a standard oscillon, can be thought of as a homoclinic orbit connecting to the trivial background state $u = 0$ in the limits $x \to \pm\infty$ as shown in Figures 9a-9b. The second localized solution, referred to as a reciprocal oscillon, can be thought of as a homoclinic orbit connecting to a nontrivial background state $u^+_{\text{unif}} \neq 0$ in the limits $x \to \pm\infty$ as shown in Figures 9c-9d. Reciprocal oscillon solutions to the CGL were originally reported in [20]. In both cases, the localized solution may have monotone or oscillatory tails. We omit discussion of the reciprocal oscillons for brevity.

Since the planar radially symmetric steady state CGL

$$0 = (1 + \mathrm{i}\alpha)\left(u_{rr} + \frac{u_r}{r}\right) + (-\mu + \mathrm{i}\omega)u - (1 + \mathrm{i}\beta)|u|^2 u + \gamma\bar{u} \tag{3.16}$$

reduces to the one-dimensional case (3.15) in the far field $r = \infty$, we expect that the bifurcation curves in one space-dimension may hold for the planar CGL. Therefore, we use the bifurcation curves for the one-dimensional CGL[1] as a starting point for our planar analysis, but with the caution that the results may not be the same. In the remainder of this chapter we review the relevant results from [2]. We remark, however, that it is not always true that the 1-dimensional results carry over to two dimensions; one therefore still needs to be precise in the analysis.

3.2.1 Spatial eigenvalue analysis

The bifurcation curves for the one-dimensional CGL were computed in [2] using a spatial eigenvalue analysis. We seek nontrivial solutions to the linearization of (3.15) about some homogeneous solution $u = u_{\text{hom}}$ of the

[1] We remark that [2] uses μ instead of $-\mu$; therefore, all bifurcation curves are flipped across the $\mu = 0$ plane relative to ours.

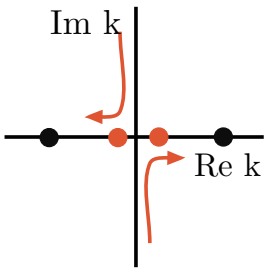

(a) *spatial eigenvalues for monotone tail solutions*

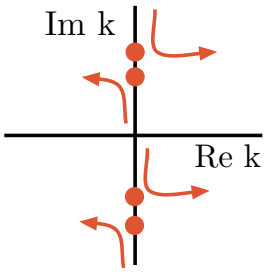

(b) *spatial eigenvalues for oscillatory tail solutions*

Figure 10: *Possible spatial eigenvalue arrangements for the bifurcation of localized solutions. Spatial eigenvalues collide on the imaginary axis and then move away.*

form $U = e^{\mathrm{i}k_j x}U_0$ where $U := (\mathrm{Re}(u), \mathrm{Im}(u))$ and U_j is the eigenvector associated with spatial eigenvalue k_j. The linearization will be of the form

$$0 = \Delta U + CU, \tag{3.17}$$

where the matrix $C := C(u_{\mathrm{hom}}) \in \mathbb{R}^2$ depends on the solution u_{hom}. Localized solutions may bifurcate as small-amplitude solutions from a homogeneous state $u = u_{\mathrm{hom}}$ only if the (3.17) has spatial eigenvalues $\{k_j\}$ with $\mathrm{Re}(k_j) = 0$ for some j. Furthermore, localized solutions bifurcate into the parameter region where these spatial eigenvalues move away from the imaginary axis: this ensures that the stable and unstable manifolds are as high dimensional as possible. Equation (3.17) has four spatial eigenvalues since there are two space derivatives and $U \in \mathbb{R}^2$; these eigenvalues obey the symmetry $k \mapsto -k$ due to the Laplacian. Thus, there are two cases to consider, as shown in Figure 10.

(i) On the bifurcation curve $k_1 = k_2 = 0$ and $k_3 = -k_4 = m \in \mathbb{R}$. Localized solutions bifurcate into the region where k_1 and k_2 split along the real axis of the complex plane; see Figure 10a. This bifurcation gives rise to localized solutions with monotone tails (Figures 9a and 9c).

(ii) On the bifurcation curve $k_1 = k_2 = \overline{k}_3 = \overline{k}_4 = \mathrm{i}m$ with $m \in \mathbb{R}$. Localized solutions bifurcate into the region where k_j split away from the imaginary axis so that $\{k_j\} \cap \mathrm{i}\mathbb{R} = \varnothing$; see Figure 10b. This bifurcation results in standard oscillons with oscillatory tails (Figures 9b and 9d).

The difference between the standard oscillons (Figures 9a and 9b) and reciprocal oscillons (Figures 9c and 9d) is that the linearization (3.17) is computed using $u \equiv 0$ and $u = u_{\mathrm{unif}} \neq 0$, respectively.

3.2.2 Standard oscillon bifurcation curves

The linearization of (3.15) about $u = 0$

$$0 = \begin{pmatrix} 1 & -\alpha \\ \alpha & 1 \end{pmatrix} \begin{pmatrix} v \\ w \end{pmatrix}_{xx} + \begin{pmatrix} -\mu + \gamma & -\omega \\ \omega & -\mu - \gamma \end{pmatrix} \begin{pmatrix} v \\ w \end{pmatrix}, \tag{3.18}$$

has four spatial eigenvalues which satisfy

$$(1 + \alpha^2)k^4 + 2(\alpha\omega - \mu)k^2 + \mu^2 + \omega^2 - \gamma^2 = 0. \tag{3.19}$$

In Figure 11 we illustrate the spatial eigenvalues k, plotted in the complex plane, for various values of ω and γ. The two bifurcation cases are as follows:

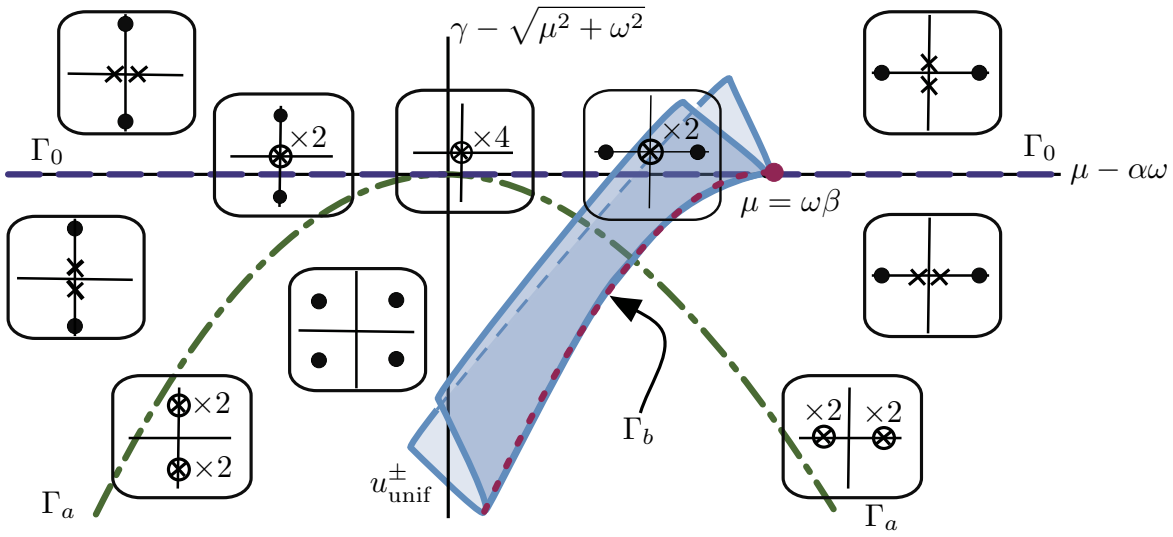

Figure 11: *Plotted is the (μ,γ)-plane with α, β, and ω fixed. The inlays are the spatial eigenvalues associated with the linearization of (3.15) about $u = 0$ plotted in the complex plane. There are two bifurcation cases to consider: (i) into the region below Γ_0 (purple dashed line) for $\mu > \alpha\omega$, and (ii) into the region below Γ_a (green dash-dotted line) for $\mu < \alpha\omega$. Non-trivial uniform solutions $u^{\pm}_{\text{unif}}$ emerge at a fold bifurcation at Γ_b (maroon dotted line); the fold curve Γ_b intersects Γ_0 at $\mu = \beta\omega$ where $u^{+}_{\text{unif}} = u^{-}_{\text{unif}} = 0$.*

(i) Define

$$\Gamma_0 := \{(\mu,\gamma) : \gamma = \sqrt{\mu^2+\omega^2}\},$$

set $\mu_m := \alpha\omega + \frac{m^2}{2}$, and pick γ_m so that $(\mu_m,\gamma_m) \in \Gamma_0$. Then, with

$$(\mu,\gamma) = (\mu_m, \gamma_m - \epsilon^2),$$

$k_{1,2}$ split into $\mathrm{O}(\epsilon)$ eigenvalues along the real axis, whilst $k_{3,4} \approx \pm m$, as shown in Figure 11. Thus, standard monotone oscillons may bifurcate for $\mu > \alpha\omega$ into the region below the curve Γ_0.

(ii) Define

$$\Gamma_a := \{(\omega,\gamma) : (1+\alpha^2)\gamma^2 = (\omega+\alpha\mu)^2\},$$

set $\mu_m := \alpha\omega - \frac{m^2}{2}$, and pick γ_m so that $(\mu_m,\gamma_m) \in \Gamma_a$. Then, with

$$(\mu,\gamma) = (\mu_m, \gamma_m - \epsilon^2),$$

$$k_j = \pm\mathrm{O}(\epsilon) \pm \mathrm{i}\big(m + \mathrm{O}(\epsilon)\big),$$

as shown in Figure 11. Thus, standard oscillatory oscillons may bifurcate for $\mu < \alpha\omega$ into the region below the curve Γ_a.

We remark that in [2] it was found that localized solution of either type only bifurcate provided that also $\mu < \beta\omega$. The same condition remains true in the planar case; it is related to a subcriticality condition.

4 Our numerical results in 2 spatial dimensions [9]

We first remark that we have proven the existence of small amplitude localized solutions in two spatial dimensions in [9]. We omit a detailed review of this result since this lecture focuses on numerical methods to find solutions far from onset.

Theorem 1 *Fix $\alpha\omega < \mu < \beta\omega$ and let $\gamma = \sqrt{\mu^2+\omega^2} - \epsilon^2$. Then there is an $\epsilon_0 > 0$ so that (3.16) has a nontrivial stationary localized radial solution of amplitude $\mathrm{O}(\epsilon)$ for each $\epsilon \in (0,\epsilon_0)$.*

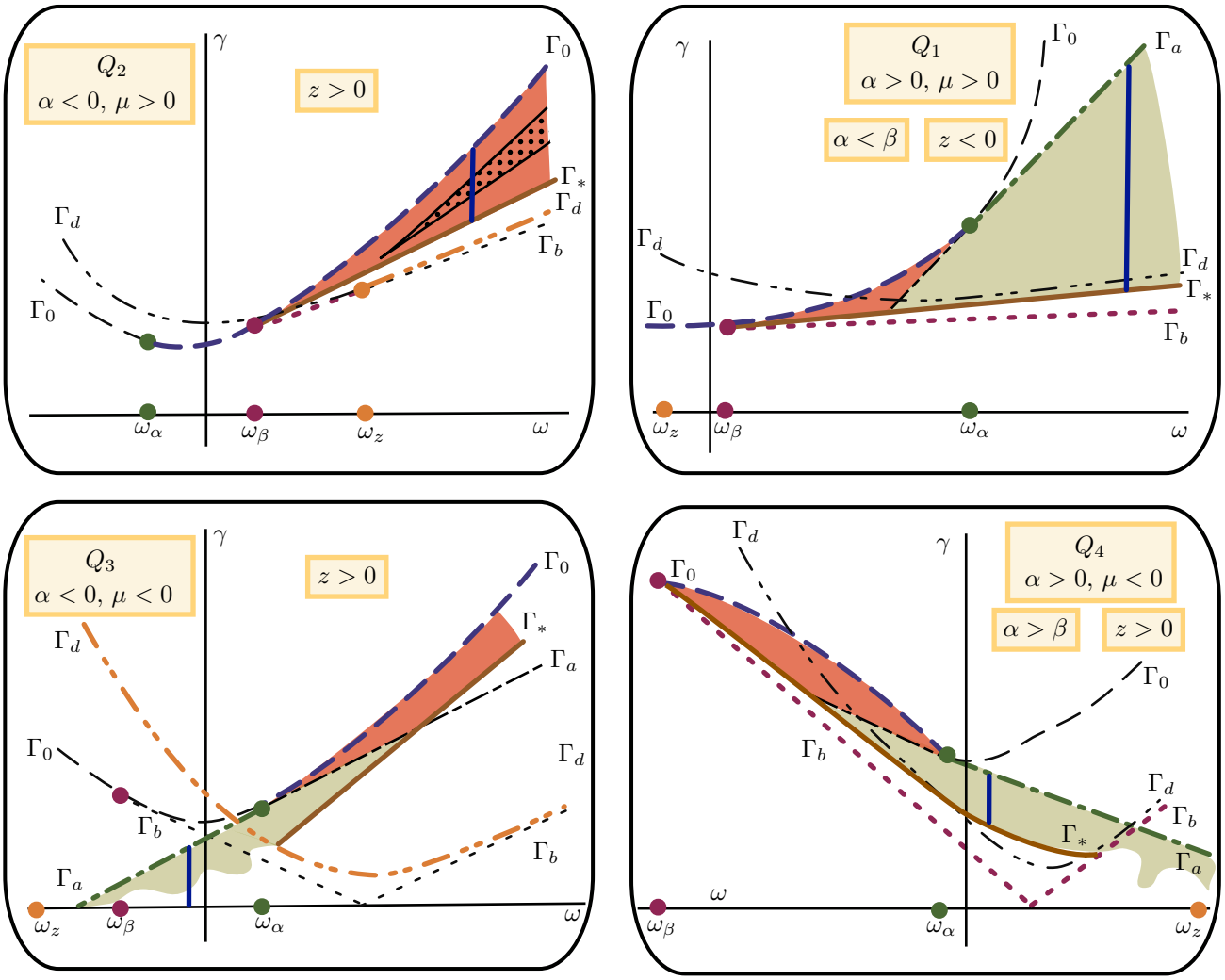

Figure 12: *Expected existence regions of standard oscillons in each of the parameter quadrants. We refer to Figure 13 for the interpretation of the curves shown here: the segments of the curves Γ_j that coincide with bifurcations are highlighted; otherwise, we use the same line style as in Figure 13, but the curve is thin and black. Small amplitude localized solutions bifurcate into the parameter region below Γ_0 and Γ_a provided that also $\omega > \omega_\beta := \mu/\beta$. The dark salmon shaded regions indicate the numerically observed existence region for localized solutions with monotone tails; the light green shaded regions indicate the existence region for localized solutions with oscillatory tails. Solutions bifurcating from Γ_0 are observed to develop oscillatory tails for $\gamma < \gamma_a$ (with the notation of (4.1)). In parameter regions Q_1, Q_2, and Q_4, all localized solutions terminate in a stationary one-dimensional front at Γ_*. In Q_3, Γ_* ends at the curve Γ_d; the termination of solutions for parameter values to the left of Γ_d in Q_3 is not well understood. Stable oscillons were found in between two saddle nodes in a small subset of Q_2.*

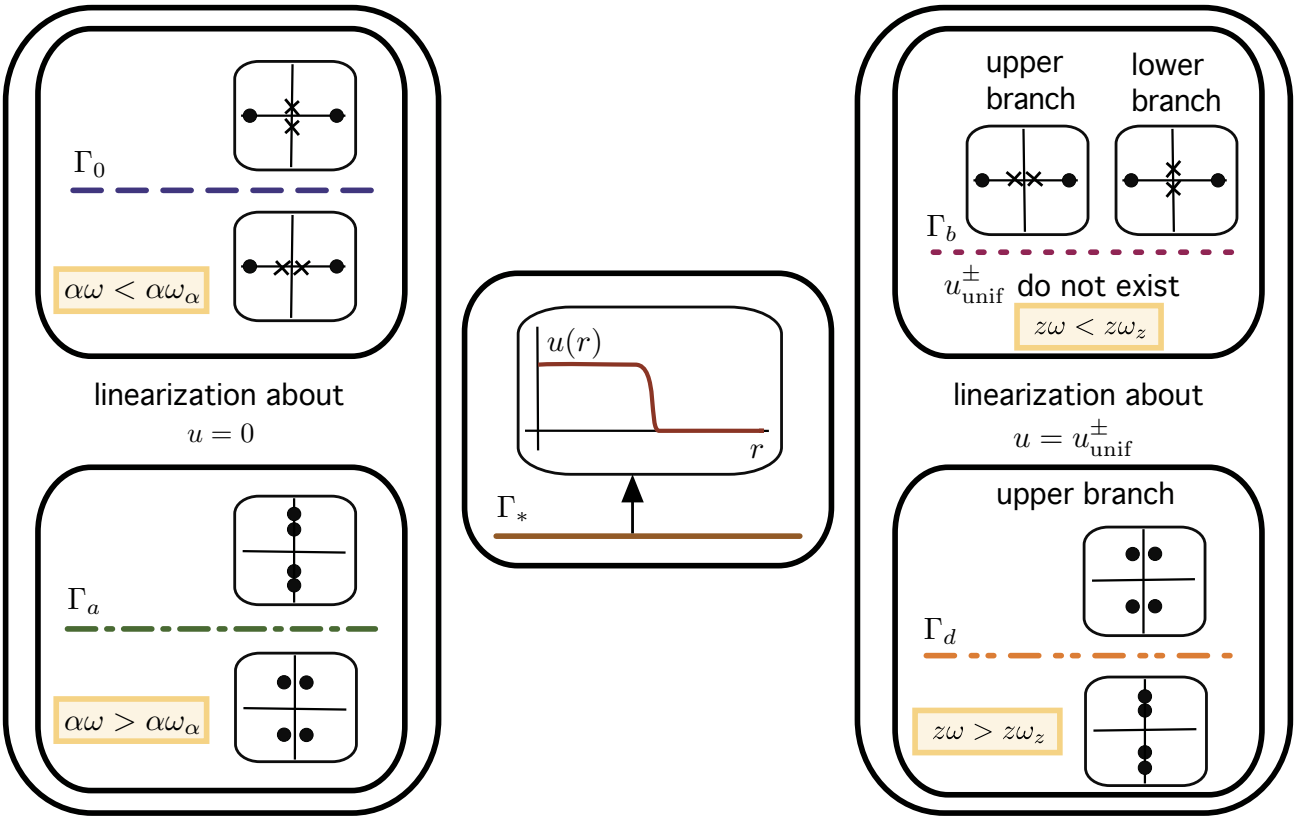

Figure 13: *Color and line style legend for the various bifurcation curves shown in Figure 12 in the* (ω, γ) *plane. The insets for* Γ_0, Γ_a, Γ_b, *and* Γ_d *represent the spatial eigenvalues of the linearization of (3.16) at* $r = \infty$ *about either* $u = 0$ *or* $u = u^{\pm}_{\text{unif}}$. *The spatial eigenvalues are shown for the parameter regions indicated; for parameter values in the opposite parameter region, the spatial spectra should be rotated by 90 degrees. The inset for* Γ_* *depicts a representative solution profile along the curve* Γ_*.

	β	α	μ	$z := \alpha(1-\beta^2) - 2\beta$
Q_1	10.0	0.5	10.0	-69.5
Q_2	2.5	-2.0	0.5	5.5
Q_3	2.5	-2.0	-0.5	5.5
Q_4	0.5	10.0	-5.0	6.5

Table 1: *Values of the fixed parameters for our numerical computations in each region.*

The requirement $\mu > \alpha\omega$ and $\gamma < \sqrt{\mu^2 + \omega^2}$ is the spatial eigenvalue condition discussed above. One can show that $\text{sign}(\mu - \omega\beta)$ equals the sign of the leading-order nonlinear term in an appropriate center-manifold reduction of (3.16) near $\epsilon = 0$. Therefore, the condition $\mu < \omega\beta$ ensures that the bifurcation from the curve $\gamma_0(\omega, \mu) = \sqrt{\mu^2 + \omega^2}$ is subcritical and leads to localized patterns. The subcriticality plays a key role in the analysis.

Our numerical results are summarized in Figure 12 below. We use the parameter values shown in Table 1 to explore several 2-parameter slices of the 5-dimensional parameter space. For each bifurcation curve Γ_j, we also define $\gamma = \gamma_j = \gamma_j(\omega)$ such that

$$(\omega, \gamma_j) \in \Gamma_j \quad \text{for all other parameters fixed.} \tag{4.1}$$

For example, $\gamma = \gamma_0$ means that $(\omega, \gamma_0) \in \Gamma_0$. We refer the reader to [9] for more details.

References

[1] H. Arbell and J. Fineberg. Temporally harmonic oscillons in Newtonian fluids. *Phys. Rev. Lett.* **85** (2000) 756–759.

[2] J. Burke, A. Yochelis and E. Knobloch. Classification of spatially localized oscillations in periodically forced dissipative systems. *SIAM J. Appl. Dyn. Sys.* **7** (2008) 651–711.

[3] P. Coullet and K. Emilsson. Strong resonances of spatially distributed oscillators: A laboratory to study patterns and defects. *Physica D* **61** (1992) 119–131.

[4] E. Doedel and B. Oldeman. AUTO07p: continuation and bifurcation software for ordinary differential equations. Technical report, Concordia University, 2009.

[5] C. Elphick, G. Iooss and E. Tirapegui. Normal form reduction for time-periodically driven differential equations. *Phys. Lett. A.* **120** (1987) 459–463.

[6] R. Hoyle. *Pattern Formation. An Introduction to Methods*. Cambridge University Press, Cambridge, 2006.

[7] O. Lioubashevski, Y. Hamiel, A. Agnon, Z. Reches and J. Fineberg. Oscillons and propagating solitary waves in a vertically vibrated colloidal suspension. *Phys. Rev. Lett.* **83** (1999) 3190–3193.

[8] K. McQuighan. *Oscillons near Hopf bifurcations of planar reaction diffusion equations*. Ph.D. thesis, Brown University, 2014.

[9] K. McQuighan and B. Sandstede. Oscillons in the planar Ginzburg–Landau equation with 2:1 forcing. Under review. `http://math.bu.edu/people/kmcquigh/papers/CGL_SSO.pdf` (2014).

[10] V. Petrov, Q. Ouyang and H. Swinney. Resonant pattern formation in a chemical system. *Nature* **388** (1997) 655–657.

[11] B. Sandstede and D. Lloyd. Using auto for stability problems. Lecture notes from workshop on "The stability of coherent structures and patterns". `http://www.dam.brown.edu/people/sandsted/auto/auto-tutorial.pdf` (2012).

[12] M. Shats, H. Xia and H. Punzmann. Parametrically excited water surface ripples as ensembles of oscillons. *Phys. Rev. Lett.* **108** (2012) 034502.

[13] P. Umbanhowar, F. Melo and H. Swinney. Localized excitations in a vertically vibrated granular layer. *Nature* **382** (1996) 1942–1945.

[14] V. Vanag and I. Epstein. Stationary and oscillatory localized patterns, and subcritical bifurcations. *Phys. Rev. Lett.* **92** (2004) 128301.

[15] V. Vanag and I. R. Epstein. Localized patterns in reaction–diffusion systems. *Chaos* **17** (2007) 037110.

[16] V. Vanag, L. Yang, M. Dolnik, A. Zhabotinsky and I. Epstein. Oscillatory cluster patterns in a homogeneous chemical system with global feedback. *Nature* **406** (2000) 389–391.

[17] V. Vanag, A. Zhabotinsky and I. Epstein. Oscillatory clusters in the periodically illuminated, spatially extended Belousov–Zhabotinsky reaction. *Phys. Rev. Lett.* **86** (2001) 552–555.

[18] J. Wu, R. Keolian and I. Rudnick. Observation of a non-propagating hydrodynamic soliton. *Phys. Rev. Lett.* **52** (1984) 1421–1424.

[19] H. Xia, T. Maimbourg, H. Punzmann and M. Shats. Oscillon dynamics and rogue wave generation in Faraday surface ripples. *Phys. Rev. Lett.* **109** (2012) 114502.

[20] A. Yochelis, J. Burke and E. Knobloch. Reciprocal oscillons and nonmonotonic fronts in forced nonequilibrium systems. *Phys. Rev. Lett.* **97** (2006) 254501.